

Identification of 1,2,4-Oxadiazoles-Based Novel EGFR Inhibitors: Molecular Dynamics Simulation-Guided Identification and in vitro ADME Studies

Vishal Unadkat^{1,2}, Shishir Rohit¹, Paranjay Parikh³, Kaushal Patel³, Vinod Sanna⁴, Sanjay Singh^{2,5}

¹Kashiv Biosciences Pvt Ltd, Ahmedabad, 382210, Gujarat, India; ²Division of Biological & Life Sciences (Formerly Institute of Life Sciences), School of Arts & Sciences, Ahmedabad University, Ahmedabad, 380009, Gujarat, India; ³Department of Advanced Organic Chemistry, P.D. Patel Institute of Applied Sciences, Charotar University of Science and Technology, Changa, Gujarat, 388421, India; ⁴Piramal Pharma Solutions, Ahmedabad, 382213, Gujarat, India; ⁵National Institute of Animal Biotechnology, Hyderabad, 500032, Telangana, India

Correspondence: Sanjay Singh, Division of Biological & Life Sciences (Formerly Institute of Life Sciences), School of Arts & Sciences, Ahmedabad University, Navaragnpura, Ahmedabad, 380009, Gujarat, India, Email sanjay.singh@ahduni.edu.in

Background: In this work, we have identified heterocyclic derivatives with 1,2,4 oxadiazole scaffold mimicking the functions of tyrosine kinase inhibitors. Fourteen molecules that displayed the best fit were picked from the library of compounds and studied under in-silico and in-vitro conditions. Four compounds were selected for further cytotoxicity and ADME (Absorption, Distribution, Metabolism, Elimination) profiling showing IC₅₀ (from 8–13 μM) values against EGFR positive cancer cell line (MCF7).

Methods: A molecular dynamics simulation study was performed to understand the correlation of non-covalent binding energies with biological activity. The drug-like properties of the selected four compounds (7a, 7b, 7e, and 7m) were evaluated by in-vitro ADME studies. Compounds 7a, 7b, and 7m were the active compounds in the molecular dynamics simulations study. Further, EGFR binding activity was confirmed with EGFR^{WT} and EGFR^{T790M} kinase assay using a luminescence-based method.

Results: These compounds (7a, 7b, and 7m) showed activity against EGFR^{WT} and mutant EGFR^{T790M}, exhibiting IC₅₀ values of <10 and <50 micromolar, respectively. These compounds also possess moderate aqueous solubility in 40–70 μg/mL at pH 7.4 and 30–100 μg/mL at pH 4.0. Further, 7a, 7b, and 7m showed balanced lipophilicity with Log D values ranging from 1–3. They demonstrated a good correlation in Caco-2 permeability with Apparent permeability (Papp) 1 to 5 × 10⁻⁶ cm/s in comparison with 7e, which was found to be highly lipophilic (Log D >5) and showed high permeability (Papp 17 × 10⁻⁶ cm/s). Lastly, all these compounds were moderately stable in liver microsomes at alkaline pH with a half-life of 30–60 min, while at a highly acidic pH (2.0), the compounds were stable up to 15–20 min.

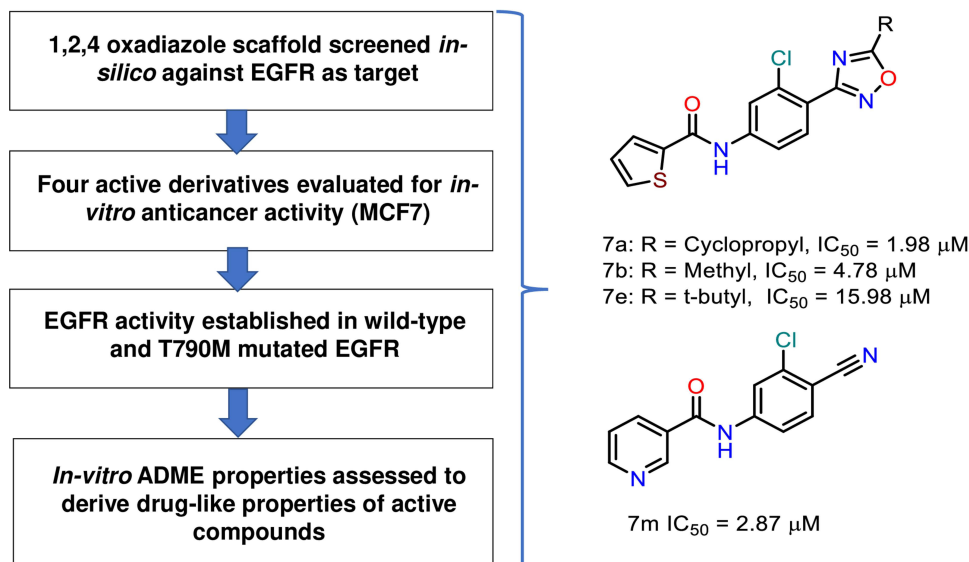
Conclusion: Overall, in-vitro ADME results of these molecules showed good drug-like properties, which are well correlated with the in-silico ADME data, making them ideal for developing an oral drug delivery formulation.

Keywords: 1,2,4-oxadiazoles, structure-based design, molecular dynamics, absorption, distribution, metabolism, excretion, anticancer

Introduction

Conventional methods of cancer treatment involve chemotherapy using cytotoxic drugs. Although these drugs successfully inhibit the proliferation of cancer cells, they display poor selectivity and high cytotoxicity to nearby cells/tissues and eventually lead to resistance. Such a kind of resistance occurs very frequently in which a treatment of any chemical drug becomes ineffective as the disease turns out to be tolerant. Several cancer types are vulnerable to chemotherapy at the beginning of the cure, while there are other cancers wherein the resistance develops over time through one or other mechanisms. Drug resistance primarily arises due to mutation in DNA which ultimately changes the metabolism and triggers inhibition and degradation of drugs.¹ Targeting the surface molecules of cancerous cells enhances the tumour specificity and efficacy of delivered drugs.²

Graphical Abstract



The Epithelial Growth Factor Receptor, more commonly known as EGFR, is a common molecular target for cancer. It controls growth factors, cell proliferation, angiogenesis, anti-apoptosis, and metastasis processes.³ The EGFR belongs to the ErbB category of receptor tyrosine kinase. Chemically, EGFR is a glycoprotein with a molecular weight of 170 kDa. It has an extracellular receptor domain, a domain with a tyrosine function located intracellularly, and an additional transmembrane.^{4,5} It is reported in the literature that EGFR and HER-2 are overexpressed in several cancer cells originating from various organs, including the bladder, breast, colon, and lungs. Thus, EGFR is one of the attractive molecular targets for treating cancer.⁶⁻⁸

Developing new drug candidates that are efficient in inhibiting protein kinases such as tyrosine kinase would be of considerable interest. Gefitinib and erlotinib are first-generation inhibitors of EGFR with similar chemical structures.⁹ Both of these molecules were very effective as chemotherapy in lung cancer treatment and explored in other cancer types. Due to significant responses from the patients with such EGFR inhibitors, efforts were made in developing second-generation EGFR inhibitors such as afatinib.¹⁰

Although there are few reports on developing EGFR inhibitors through various mechanisms,¹¹ they display poor efficacy when investigated to inhibit the proliferation of cancer cells.^{12,13} Many known kinase inhibitors, i.e. gefitinib, lapatinib, pazopanib, ponatinib, sunitinib, showed good efficacy; however, the side effects of elevated liver enzymes, skin rash, and interstitial pneumonia were found to be a significant limitation of such molecules during clinical trials.¹⁰ The other issues with most of the kinase inhibitors are higher molecular weight and lipophilicity,¹⁴ limiting their aqueous solubility and cell permeability,¹⁵ thus resulting in poor toxicity to cancer cells.¹⁶ Effective kinase inhibitors are expected to have a high kinase selectivity^{17,18} and lower side effects on nearby tissues.¹⁹ Moreover, it is reported that patients on drugs such as EGFR inhibitors also at a later stage receive chemotherapeutic treatment, which, in turn, may make them prone to severe side effects, including organ failure.²⁰ Therefore, it is essential to address ADME (Absorption, Distribution, Metabolism, Elimination) issues at an early stage of drug discovery to avoid any setbacks at a later stage.

In silico molecular design is one of the widely used methodologies that help drug discovery scientists save time and money by focusing their efforts rationally. Many success stories of drugs being discovered using these approaches are

reported in the literature.^{21,22} For developing EGFR inhibitors, a virtual screening method has been used to shortlist the best pharmacophore from the library of 1500 compounds.^{11,23}

One of the promising methodologies in structure-guided drug design is molecular docking. It helps in understanding of potential interactions between a small or large molecule (ligand) and the macromolecular target (protein of interest). The process involves sampling the ligand over a sizeable conformational space to identify the possible binding geometry of the binding pose. Based on the binding pose's favourable interactions with the target protein, i.e., H-bonding interactions, Van der Waals interactions, lipophilic interactions, halogen bonding, and other non-covalent interactions, the binding energy is predicted in terms of binding score (dock score). Along with structure-based drug design, the ADME assessment has equally essential aspects. It is well known that many drug candidates fail in the advanced stages of drug discovery, i.e., the clinical phase, due to not having good drug-like properties. Therefore, early assessment of in-silico and in-vitro ADME is crucial.

Our previous study screened a library of heterocyclic molecules and identified a set of fourteen molecules exhibiting EGFR inhibition.^{24,25} In this study, we have performed a molecular docking study on all the fourteen compounds that revealed the four most active compounds/molecules. Finally, these four compounds were chosen for molecular dynamics study and ADME profiling to understand their drug-like properties.

Materials and Methods

Materials

Mol soft (ICM Version 3.9-2C/Win), GROMACS version 2019.4 (amber 14sb force field), ACPYPE (AnteChamber PYthon Parser interface) program, Grace 5.1.22 and QtGrace version 2.6 software were used for all in-silico activities. MCF7 and MRC5 cell lines were used from ATCC; LDH Cytotoxicity Assay Kit, Item No. 601170 was used from Cayman Chemical; EGFR Kinase assay kit, Catalogues no. 40321 and 40323 were used from BPS Bioscience; Caco-2 (human colon carcinoma) cell line, borrowed from NCCS, Pune; which was initially procured from American Type Culture Collection (ATCC). All other chemicals, solvents, and reagents were procured commercially.

Methods

Chemical Synthesis and Structure

We have previously reported the synthesis of a series of heterocyclic compounds having 1,2,4-oxadiazole scaffold (Figure 1),²⁴⁻²⁶ which was obtained by reaction of 4-amino-2-chlorobenzonitrile (**1**) with respective acid chloride (**2**). The reaction was carried out using triethylamine (TEA) as a base to afford the target amide (**3**). The reaction of hydroxylamine (**4**) with compound (**3**) afforded benzetimide analogues (**5**). Finally, the microwave-assisted reaction of respective carboxylic acids (**6**) with compound (**5**) afforded target final compounds (**7**) (60–80% yield). The structures of the synthesized compounds are summarized in Table 1.

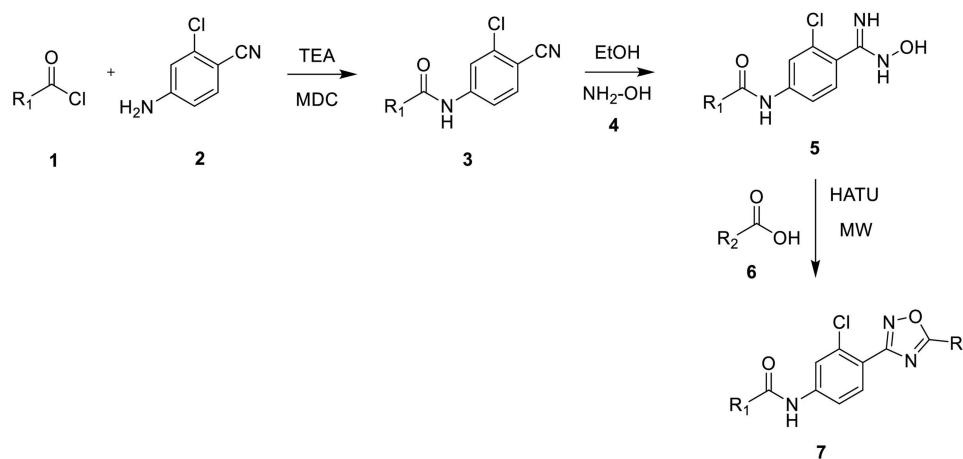


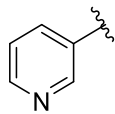
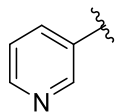
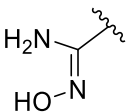
Figure 1 Synthetic pathway of 3,5-disubstituted-1,2,4-oxadiazoles (**7**).

Table 1 Structures of Fourteen Synthesized Derivatives Along with Their Docking Results

General Structure of Target Compounds	Target Compound	R ₁	R ₂	Dock Score
	7a			-15.1
	7b			-16.1
	7c			-9.5
	7d			-9.7
	7e			-10.2
	7f		CN	-7.3
	7g			-8.3
	7h			-3.9
	7i			-9.2
	7j			-7.4
	7k			-8.0
	7l			-7.2

(Continued)

Table I (Continued).

General Structure of Target Compounds	Target Compound	R ₁	R ₂	Dock Score
	7m		CN	-8.6
	7n			-8.6

Molecular Docking

We used Molsoft software (ICM version 3.8–7c) to conduct molecular docking studies. For docking studies, the final pose of the MD run was used. Other parameters were kept at default, including the removal of water molecules. Ligand structures were drawn in the sketch module of ICM, converted to 3D structures, and then minimized. The grid was set up around the following residues, which make the binding site: M793 (hinge region), F856, L777, C775, T854, T790, L788, and M766. All the other parameters were kept as default.

Molecular Dynamics (MD) Study

We evaluated four ligands (highest, moderate, and most minor scoring) for their stability and change in interaction within the active site using molecular dynamics (MD) simulation. These four compounds were selected based on their docking scores and protein-ligand interactions published in our previous publication.²⁵ For this study, we used a high resolution (1.5 Å) crystal structure of the EGFR (wild type) kinase domain (PDB Code 3POZ). MD simulation studies of EGFR protein with four ligands (highly active **7a** and **7b**, moderately active **7m**, and least active **7e**) were carried out using GROMACS version 2019.4. Ligand topologies were generated using the ACPYPE program. The protonation state of the titratable amino acids was not evaluated before MD simulation and was kept at default. However, the overall system was neutralized by adding appropriate counter ions during one of the MD simulations steps. The ligand topology was generated by ACPYPE (based on ANTECHAMBER), and parameters were assigned according to the AMBER force field. AM1 BCC option was used to determine the partial atomic charges. TIP3P water model was used at 1 Å with dodecahedron water as solvent. Neutralization of the system was made using suitable ions. We used the particle mesh Ewald method for the initial simulation, which was used for the distant-range electrostatic interaction. The nonbonding cut-off was made at 8 Å. Steepest descent method was used for the minimization to get rid of unfavourable contacts. The minimized system was subjected to Canonical ensemble (NVT) equilibration using a Langevin thermostat. The experiment was performed for 500 ps with a temperature of 0–300 K at a constant volume. Subsequently, isothermal–isobaric (NPT) equilibration was carried out with a temperature of 300 K using a Berendsen thermostat with constant pressure. We started the production steps using the NPT ensemble when the temperature achieved 300 K, followed by the final run for 20 ns. The trajectories were recorded for each ps and used to obtain a deeper understanding of the stable conformation of the protein-ligand complex. To maintain hydrogen bonds throughout the simulation, SHAKE algorithm²⁷ was used. The MD study was subjected to 20 ns. We also calculated several parameters, i.e., root means square fluctuation (RMSF), hydrogen bonding interactions, the radius of gyration (Rg), and root mean square deviation (RMSD).

Cell Culture Studies

Cytotoxicity of the compounds was tested on MCF7 and MRC5 using an LDH (Lactate Dehydrogenase) assay kit (catalogue no. 601170, Cayman Chemical, MI, USA). TAK-285 and erlotinib were used as reference controls as known EGFR inhibitors. 1×10^4 cells/well were incubated with seven different concentrations of test compounds and reference compounds at 100, 30, 9.02, 2.71, 0.81, 0.24 and 0.07 μM along with vehicle control (0.5% DMSO) substances at 37 °C in CO₂ incubator. The culture supernatant (5 μL) was isolated and incubated with an LDH test reaction mixture for 30

min at 37 °C. The OD at 490-nanometer wavelength was measured via a multimode plate reader. IC₅₀ was determined using GraphPad prism software for the test and control compounds.

In vitro EGFR Kinase Inhibition Test

Using erlotinib as a reference standard control, four potential candidates (**7a**, **7b**, **7e**, and **7m**) were investigated for EGFR kinase inhibitory activity. All the assay steps were followed as described in EGFR^{WT} and EGFR^{T790M} Kinase Assay Kit Catalogue no. 40321 and Catalogue no 40323, respectively (BPS Biosciences, CA, USA). Briefly, 5x Kinase Buffer 1, ATP and PTK substrate Poly (Glu: Tyr 4:1) (10 mg/mL) was thawed and master mixture (25 µL per well) was prepared with 6 µL 5x Kinase Buffer 1 + 1 µL ATP (500 µM) + 1 µL PTK substrate Poly (Glu: Tyr 4:1) (10 mg/mL) + 17 µL water. For initiation of the reaction, 25 µL of a master mixture, 5 µL of inhibitor solution, and 20 µL of EGFR enzyme were added per well. A positive control reaction was kept with buffer (without inhibitor) and the same amount of enzyme, while the blank reaction was kept with kinase buffer in the absence of enzyme. All the reaction samples were incubated at 30 °C for 40 minutes, and then 50 µL of Kinase-Glo Max reagent was added to each well, followed by 15 min incubation at RT in a dark condition. At the end of incubation, the luminescence was measured, and the % inhibition values at each concentration were calculated considering the positive control response as 100%. Further, the IC₅₀ values were determined using GraphPad prism software.

Thermodynamic Solubility

Our target compounds (1000 µg/mL) were dissolved in sodium phosphate buffer saline (PBS) at physiological pH and another buffer (sodium acetate) at pH 4.0. Then, the reaction mix was incubated at room temperature on RotoSpin (shaker) at 50 rpm for 24 h. Next, the solution was filtered using 0.45-micron PVDF filters, and the filtrate was used for quantification using a UV-Vis spectrophotometer (Omega Polar Star, BMG Labtech). Serial dilution was prepared to make a calibration curve to quantify the unknown concentrations of the compounds. A UV-Vis spectrophotometer scanned samples of 1 millimolar (in DMSO) concentrations.

Log D_{7.4} Shake Flask Assay

The test compounds (2 mM in DMSO) were serially diluted in octanol to construct the standards. The area for each standard sample was analyzed using LCMS/MS and plotted vs concentration to obtain a calibration curve. The organic to aqueous ratio was kept at 1:1. Test compounds (1 mg/mL) were mixed, and the reaction mixture was stirred at 25 °C for 4 h. The organic and aqueous phases were then separated, and the target compounds were measured using LC-MS/MS. The below equation was used to determine the Log D value.

$$\text{LogD}_{7.4} = \text{Log}_{10} (\text{Conc. of a test compound in Octanol}/\text{Conc. of a test compound in PBS}).$$

Caco-2 Permeability Assay

Trans-well inserts kept in 24-well plates were used to seed 80,000 Caco-2 cells per well, maintained for 18–21 days in a culture medium to enable differentiation. Media change was given every alternate day using a suitable nutrient medium. Assay buffer having calcium and magnesium with 10 mM HEPES was prepared with pH 7.4. D-Glucose (25 mM) was added to the assay buffer. The final concentration of test compounds (10 micromolar) in the reaction system was achieved by two-fold and 100-fold intermediate stock solutions in assay buffer and DMSO, respectively. The organic content of the final drug preparation was kept at less than 1% v/v. Ten µM of test solution was prepared in the assay as mentioned earlier. Two washes were given to the Caco-2 monolayer using the assay buffer. A volt-ohm meter (hand-held instrument) was used to measure Trans Epithelial Electrical Resistance (TEER) values to check the integrity of the monolayer. Aliquots of 0.4 mL donor solution (assay buffer containing test compound) and 0.8 mL of receiver solutions (assay buffer) were added to donor and receiver compartments. It was then incubated for 2 h at 37 °C. With identical experimental conditions, control compounds with propranolol (high permeable) and atenolol (Low Permeable) were performed in separate wells. The study samples were analyzed under LCMS/MS (API-4000 – Sciex, Nexera – XR UHPLC system – Shimadzu), and the Apparent permeability (Papp) was determined using the formulas below:

$$\text{Apparent Permeability} = (\text{Volume in the acceptor well}/\text{Surface area of the membrane} * \text{Total transport time in seconds})$$

* (concentration of drug in acceptor compartment/concentration of drug in donor compartment).

Finally, the Lucifer Yellow (LY) test was performed by adding 400 μL of LY (10 μM) to each well in the filter plate. On the receiver side, 800 μL of assay buffer was kept, and the reaction was carried out at 37°C for 60 min. Samples were collected from the basolateral compartments to measure fluorescence endpoints using 485 nm and 530 nm as excitation and emission filters. The % Lucifer yellow permeation was calculated using the below equation.

$$\frac{[(\text{Relative fluorescence units (test)} - \text{Relative fluorescence units (blank)}) / \text{Relative fluorescence units (equilibrium)} - \text{Relative fluorescence units (blank)}] * 100}{}$$

Where, Relative fluorescence units (equilibrium) = Relative fluorescence units of assay buffer containing 1 μM Lucifer yellow.

Plasma Stability Assay

Plasma stability assay was performed at a 5 μM concentration of the test compound prepared from 10 mM main stock in DMSO. The test sample was incubated, and blood plasma (from humans and mice) was incubated at 37 °C for various time points. The reaction was terminated using a suitable organic solvent in chilled conditions; the samples were withdrawn at 0, 15, 30, 45, and 60 min and processed with an organic solvent containing internal standards. The analysis was performed using triple quad LC-MS/MS. The per cent compound remaining at each time point was calculated compared with the 0 min sample.

Microsomal Stability Assay

Liver microsomes from humans and mice (0.5 mg/mL) were pre-incubated in DPBS (pH 7.4 for 5 min) followed by spiking of the test compound (1 μM). Subsequently, NADPH (1 mM) was co-incubated under shaking conditions at 37 °C. Reaction was stopped using chilled acetonitrile containing internal standard. The samples were withdrawn at 0, 15, 30, 60, and 120 min for analytical processing and analysis by LCMS-MS. Obtained raw data were analyzed using GraphPad prism software to calculate 50% degradation of test compounds, and half-life values were derived. The control compound's reaction was kept in the absence of NADPH co-incubation for 0 min and 60 min time points. The DMSO was used to prepare blanks.

Chemical Stability Assay

Chemical stability assay was performed at a 5 μM concentration of the test compound prepared from 10 mM main stock in DMSO. The test sample was incubated with a buffer of highly acidic pH (2.0) and highly alkaline pH (10.0) and incubated at 37 °C for various time points. The reaction was terminated using a suitable organic solvent in chilled conditions; The samples were withdrawn at 0, 15, 30, 45, and 60 min and processed with an organic solvent containing internal standards. The analysis was performed using triple quad LC-MS/MS. The percent compound remaining at each time point was calculated compared with the 0 min sample.

Results

Molecular Dynamics Study

The MD simulation was performed in the active site over the simulation time to have insights into the conformation and stability of the target compounds in the protein. **Figure 2** shows RMSD for the EGFR (backbone atoms). RMSD deviation was observed at max (0.275 nm) in **7m** at 15 ns, attributed to the conformational change near loop and hinge regions. The conformational difference of simulated proteins with the reference shown in **Figure 3** could be because the helix region is also near the hinge and loop regions.²⁸ In the physiological system, protein and ligands are expected to interact, causing a change in protein conformation and leading to fluctuation, determined by the system's overall stability. A tightly bound protein-ligand system that is majorly enthalpy driven (by Vander Waals, hydrophobic, and H-bonds interactions) is less prone to fluctuation. Therefore, we studied the RMSF plot of different interacting residues, as shown in **Figure 4**. This study was performed for each protein (EGFR)-ligand (**7a**, **7b**, **7c**, and **7m**) complex backbone atom during a 20 ns MD simulation. Subtle differences in RMSF among the complexes were observed over the simulation, which indicates the residue's flexibility (loop region). The ligand molecule is trying to adopt a stable conformation giving an induced-fit effect, as shown in **Figure 5**. During the MD study, the radius of gyration, also known as radgyr, indicates the compactness of the protein-ligand complex. Radgyr of the EGFR-ligand system was determined, which ranged from 2.03–2.09 nm (average value 2.05 nm). A significant deviation was found in the 7e-protein complex

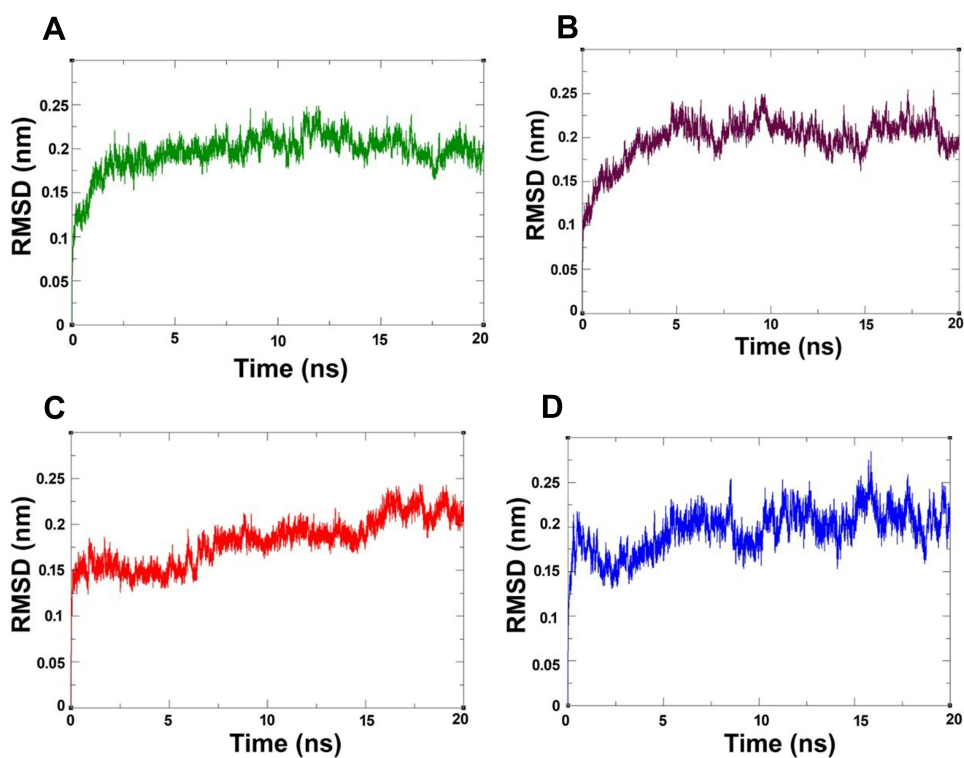


Figure 2 RMSD plot of EGFR-target compounds (backbone atoms) (A) EGFR-7a complex, (B) EGFR-7b complex, (C) EGFR-7e complex and (D) EGFR-7m complex.

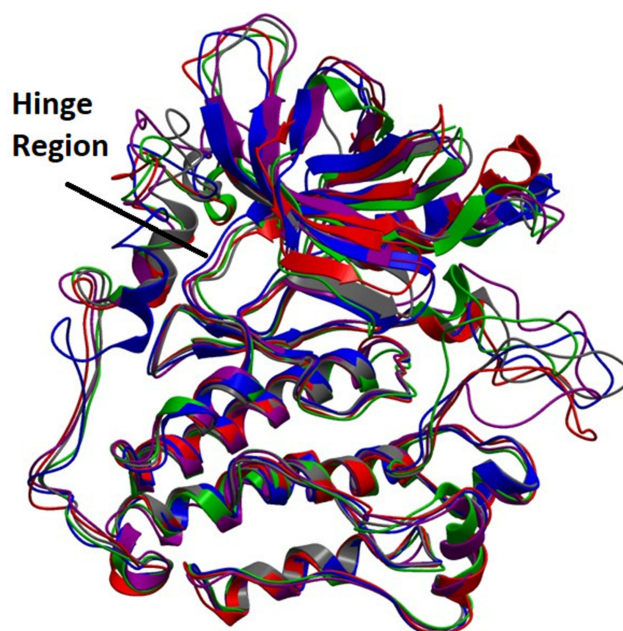


Figure 3 Conformational difference of hinge and loops with reference (black), green (7a), marron (7b), red (7e), and blue (7m).

ranging from 2.03–2.07 nm (10–15 ns), indicating a slight change in the shape (Figure 6). Hydrogen bonding interaction of the protein-ligand complex revealed that 7a and 7b shows four-hydrogen bonding interactions. However, these interactions in 7a were retained for a more extended period than 7b, which is concurrent with our experimental data, where we observed better activity in 7a. Compound 7e shows the minor activity, which could be attributed to it forming

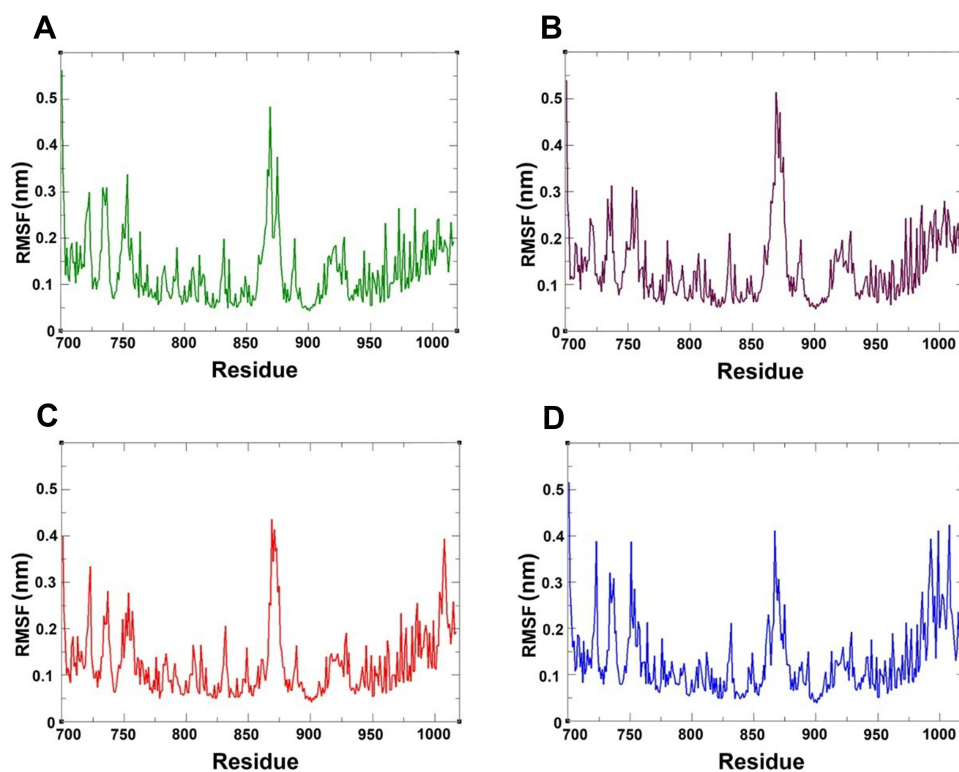


Figure 4 RMSF plot of EGFR-ligand complexes (α atoms) (A) EGFR-7a complex, (B) EGFR-7b complex, (C) EGFR-7e complex and (D) EGFR-7m complex.

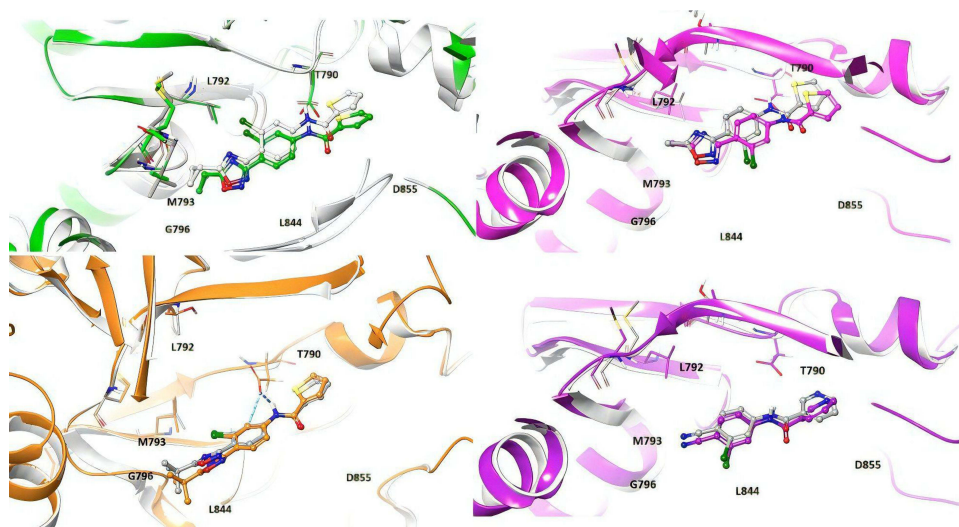


Figure 5 Initial docked poses of reference (grey colour for each EGFR-ligand complex) and overlay of MD simulated poses of corresponding EGFR-7a (green colour), EGFR-7b (marron colour), EGFR-7e (red colour), and EGFR-7m (blue colour) complexes showing induced-fit effect.

lesser hydrogen bonds with EGFR, as revealed by MD studies. The graphs for hydrogen bonding interactions are shown in Figure 7.

Breast Cancer Cell Viability Test

The cell viability was estimated using Lactate Dehydrogenase (LDH) release assay. Due to the plasma membrane damage, the LDH enzyme releases out from the cytoplasm. We used two cell lines to determine cell viability: (a) MCF7

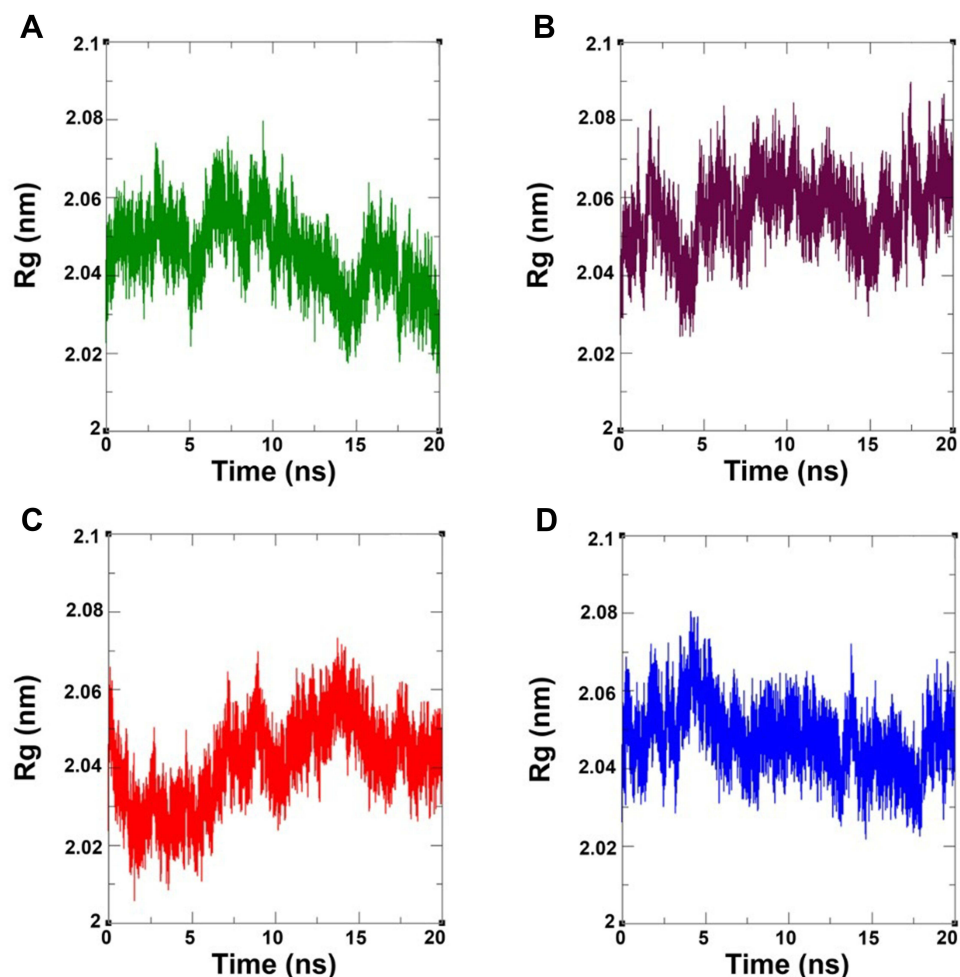


Figure 6 Radius of gyration of EGFR-ligand complexes (A) EGFR-7a complex, (B) EGFR-7b complex, (C) EGFR-7e complex, and (D) EGFR-7m complex.

(EGFR positive cancer cell line) and (b) MRC5 (normal fibroblast cells from lungs without EGFR expression). Different concentrations of identified compounds **7a**, **7b**, **7e**, and **7m** were subjected to these cell lines from 100 μM as the highest concentration and then 3.33-fold serial dilution up to 7 points with 0.07 μM as the lowest concentration. IC_{50} values of all tested compounds (**7a**, **7b**, **7e**, and **7m**) were calculated (Figure 8). All four compounds have lower IC_{50} values of 9.56 ± 2.33 , 11.98 ± 3.76 , 13.12 ± 2.98 , and 8.66 ± 2.57 for **7a**, **7b**, **7e**, and **7m**, respectively, than the control EGFR inhibitors (TAK-285 and erlotinib with IC_{50} values of 15.46 ± 5.6 and 18.54 ± 4.9 μM , respectively) in MCF7 cell line confirming their role as EGFR inhibitors. Further, compounds **7a**, **7b**, **7e**, and **7m** and reference control compounds exhibited $\text{IC}_{50} > 30$ μM in MRC5, reinforcing the specificity towards EGFR inhibition by not affecting healthy lung fibroblast cells. **7a** and **7m** showed more promising results in the MCF7 cell line among the tested compounds.

In vitro EGFR Kinase Inhibitory Assay

EGFR^{T790M} is a prominent mutation in EGFR, seen in nearly half of lung tumours that showed EGFR mutations.²⁹ The EGFR kinase inhibition test was carried out for two kinase enzymes: (a) EGFR (EGFR^{WT}, wild-type) and (b) EGFR^{T790M} (EGFR-mutated at 790 residues) using an EGFR kinase assay kit. Test compounds had significant inhibitory potential on wild-type EGFR but not against the mutant EGFR (Figure 9). The results indicated that **7a**, **7b**, and **7m** might result in potential therapeutic targets considering lower micromolar IC_{50} values of 1.98 ± 0.69 , 4.78 ± 1.23 , and 2.87 ± 1.12 μM , respectively, in EGFR^{WT} kinase. At the same time, compound **7e** has shown relatively more minor inhibition of EGFR

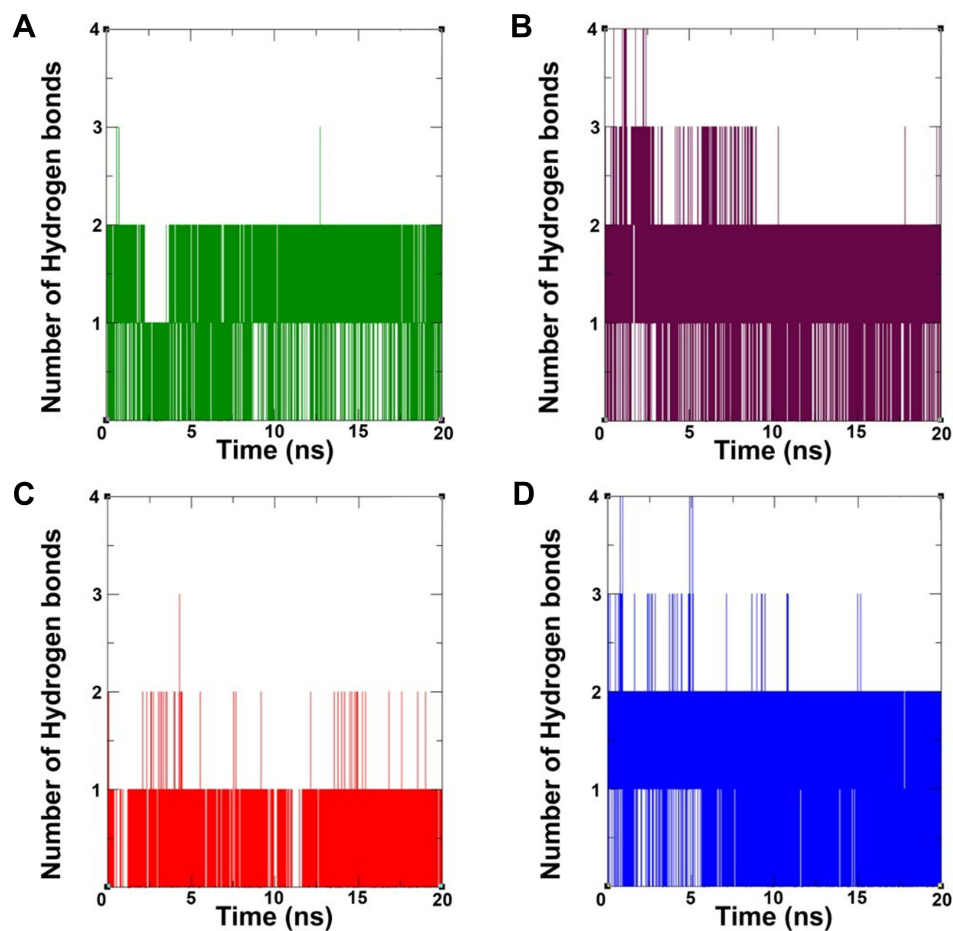


Figure 7 Number of hydrogen bonds in EGFR-ligand complexes; (A). EGFR-7a complex, (B) EGFR-7b complex, (C) EGFR-7e complex and (D) EGFR-7m complex.

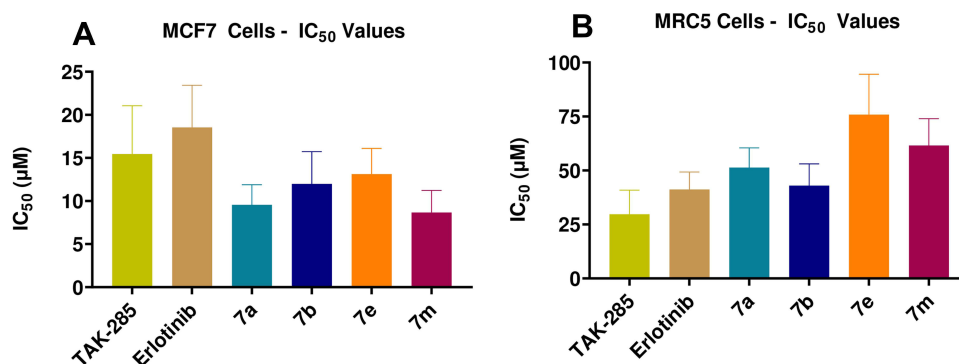


Figure 8 IC_{50} determination in (A) MCF7 and (B) MRC5; Three independent experiments were performed, and mean \pm standard deviation was reported; GraphPad Prism software was used to calculate IC_{50} values.

activity with an IC_{50} value of $15.98 \pm 4.87 \mu\text{M}$. Further, all four compounds showed $> 25 \mu\text{M}$ IC_{50} in EGFR^{T790M} kinase, indicating selectivity towards EGFR^{WT} kinase inhibition.

Solubility of Compounds

Compounds with poor aqueous solubility result in compromised therapeutic efficacy and unfavourably affect the pharmacokinetic and pharmacodynamic properties of the therapeutic compounds. Therefore, the thermodynamic solubility test of a compound could provide important information about the compounds' suitability for biological

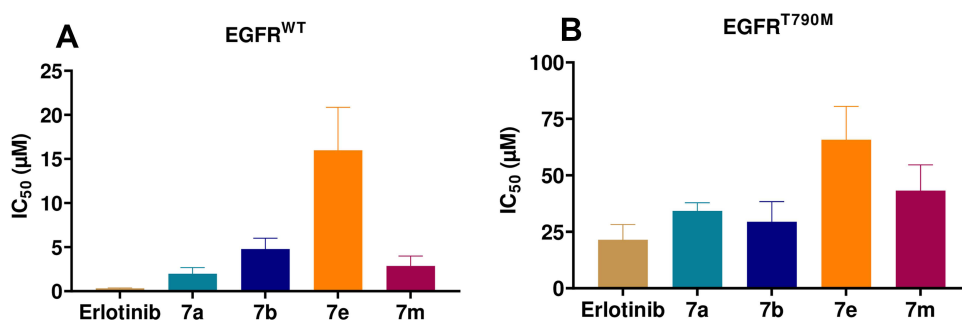


Figure 9 IC₅₀ determination from EGFR kinase activity assay in (A) EGFR^{WT} and (B) EGFR^{T790M}; Data represented as mean ± standard deviation; N = 3, GraphPad Prism software was used to calculate IC₅₀ values.

applications.³⁰ All the four tested compounds showed moderate solubility at pH 7.4 but better solubility at pH 4.0 (Table 2). The aqueous thermodynamic solubility of **7a**, **7b**, and **7e** at pH 7.4 was found to be 45.9 ± 7.2 , 56.6 ± 9.5 , and 67.8 ± 6.4 µg/mL, respectively. At the same time, **7m** was soluble up to 39.3 ± 5.8 µg/mL concentration, which is relatively lower than **7a**, **7b**, and **7e**. A similar solubility trend was observed at pH 4.0, where **7a**, **7b**, and **7e** showed relatively higher solubility with 130 ± 19 , 97.3 ± 9.5 , and 45.3 ± 8.4 µg/mL compared with **7m** which has demonstrated solubility of 27.6 ± 2.1 µg/mL. Reference compounds albendazole and quinidine were kept as QC control of the assays from each category (low and high soluble reference). Accordingly, albendazole having low solubility, showed <1 µg/mL solubility at the tested pH (4.5 and 7.4). At the same time, quinidine was taken as a highly soluble reference and was soluble at pH 7.4 and pH 4.5 with >0.45 mg/mL and >1 mg/mL, respectively. These results suggest that the compounds could be developed as orally administered compounds to promote intestinal absorption.

Lipophilicity of Compounds

The distribution coefficient (Log D) is widely used to assess the lipophilicity of compounds. Octanol buffer shake flask assay is a universally accepted way of determining Log D, where the test compound is being partitioned between two systems, i.e., octanol and aqueous buffer. The excellent Log D value for an oral drug candidate ranges between 0–5 (Lipinski's rule of 5), which, in turn, shows a reasonable balance between permeability and solubility.³¹ It was encouraging to see that the Log D values of **7a**, **7b**, and **7m** followed Lipinski's rule (Table 3).

As evident from Table 3, the obtained Log D range for these three molecules was suitable for oral delivery with sufficient permeability. Compound **7e** was highly lipophilic, which can create issues such as excessive binding with plasma proteins and vulnerability to metabolic enzymes (high clearance); which, in turn, may lead to undesirable problems in early-stage pre-clinical safety assessment assessment.³²

Table 2 Aqueous Thermodynamic Solubility of Test Compounds

Compound ID	Thermodynamic Solubility (µg/mL)	
	pH 7.4	pH 4.0
7a	45.9 ± 7.2	130.1 ± 19.1
7b	56.6 ± 9.5	97.3 ± 9.5
7e	67.8 ± 6.4	45.3 ± 8.4
7m	39.3 ± 5.8	27.6 ± 2.1
Albendazole	0.72 ± 0.2	0.91 ± 0.1
Quinidine	479.2 ± 22.1	1119.3 ± 43.1

Note: Data represented as mean ± standard deviation; N = 3.

Table 3 Lipophilicity of the Test Compounds

Compound ID	Log D _{7.4}
7a	4.3 ± 0.6
7b	3.3 ± 0.4
7e	>5
7m	1.9 ± 0.3
Albendazole	3.6 ± 0.1
Furosemide	-0.5 ± 0.1

Note: Three independent experiments were performed, and the mean ± standard deviation was reported.

Stability of Compounds in Plasma

It is well known that assessing the stability of drug candidates in plasma is crucial as many compounds undergo metabolism in plasma by an enzymatic pathway. Plasma stability can result in a high clearance leading to a short half-life for compounds, especially those administered parenterally.³³ Hence, plasma stability is performed to assess the groups susceptible to hydrolysis in plasma. Propantheline bromide was used as a reference compound which showed 50% degradation within 30 min in both the tested species of plasma, indicating the system is suitable for testing compounds. All the test compounds (**7a**, **7b**, **7e**, and **7m**) were stable; their half-life was found to be >120 min (human plasma). In mouse plasma, compounds **7a** and **7b** showed a half-life of 89 ± 15 and 78 ± 16 min, respectively. Test compounds and **7m** were more stable in mouse plasma with a half-life of 103 ± 22 and >100 min, respectively, indicating the compounds are non-susceptible for degradation in plasma (Table 4). Such stability in the plasma matrix would help during pre-clinical and clinical pharmacokinetics studies by ensuring negligible ex-vivo degradation during analysis.

In-vitro Intrinsic Clearance Using Liver Microsomes

Phase-1 metabolism is the primary route of drug metabolism, which predominantly occurs in the liver. The majority of approved drugs undergo CYP-induced metabolism in the liver. Hence, early in-vitro intrinsic clearance assessment using liver microsomes is the key to rational drug development. Approximately 60% of marketed compounds are cleared by hepatic CYP-mediated metabolism. In vitro, intrinsic clearance obtained out of the liver microsomes is one of the most widely accepted methods to determine the vulnerability of test compounds towards phase-1 metabolizing enzymes.³⁴ Verapamil was used as the high clearance reference compound in both the species, which showed a half-life of 16.87 ± 0.38 and 8.73 ± 0.86 min in human liver microsomes (HLM) and mouse liver microsomes (RLM), respectively. Compounds **7a**, **7b**, and **7m** were degraded in human liver microsomes with a half-life of 29.43 ± 5.32, 38.43 ± 4.81, and 26.12 ± 7.54 min, respectively, indicating moderate stability and possible metabolism by phase-1 enzymes. Compound **7m** was relatively more stable with a half-life of 56.78 ± 11.32 min. In mouse liver microsomes, **7a**, **7e**, and **7m** were rapidly degraded with a half-life of 16.34 ± 3.91, 19.34 ± 6.25, and 11.65 ± 4.2 min, respectively, indicating faster metabolism in lower species. At the same time, **7b** showed moderate stability with a half-life of 41.43 ± 9.32 min. Further, **7e** was stable in HLM with a $t_{1/2}$ of ~1 hour but metabolized in mouse liver microsomes within 20 minutes, indicating species-specific metabolism (Table 5).

Table 4 Plasma Stability of Test Compounds

Compound ID	Plasma Stability - Half-Life (Minutes)	
	Human Plasma	Mouse Plasma
7a	>120	89.3 ± 15.1
7b	>120	103.2 ± 22.1
7e	>120	78.2 ± 16.1
7m	>120	>120
Propantheline bromide	29.6 ± 4.2	26.5 ± 5.6

Note: Data represented as mean ± standard deviation; N = 3.

Table 5 Liver Microsomal Stability of Test Compounds

Compound ID	Liver Microsomal Stability - Half-Life (Minutes)	
	HLM ($T_{1/2}$)	MLM ($T_{1/2}$)
7a	29.4 ± 5.3	16.3 ± 3.9
7b	38.4 ± 4.8	41.4 ± 9.3
7e	56.8 ± 11.3	19.3 ± 6.3
7m	26.1 ± 7.5	11.7 ± 4.2
Verapamil	16.9 ± 0.4	8.7 ± 0.9

Notes: Data represented as mean ± standard deviation; N = 3, Half-life determined using one-phase exponential decay parameter by GraphPad prism software.

Chemical Stability

Apart from enzymatic pathways, it is also essential to assess the drug candidate's vulnerability to chemical-induced metabolism, including various chemical transformations such as oxidation, hydrolysis, and photodegradation. The drug candidate should be chemically stable to be assessed without any stability issues in biologically relevant media, and the in vitro biological activity can be determined with accuracy.³⁵ Hence, all four compounds were tested at two sets of pH: (a) pH 2.0 (acidic) and (b) pH 10.0 (alkaline). All tested compounds were found to be moderately stable at alkaline pH with half-life values of 52.65 ± 12.4 , 46.10 ± 8.3 , 34.34 ± 7.3 , and 39.21 ± 8.7 min for **7a**, **7b**, **7e**, and **7m** respectively; however, the stability of **7a**, **7b**, **7e**, and **7m** at highly acidic pH was found to be low with a half-life of 15.23 ± 5.2 , 26.16 ± 7.5 , 10.41 ± 5.7 , and 21.21 ± 7.3 , respectively suggesting labile availability groups for acidic degradation. **7b** was relatively stable out of our four compounds at acidic pH 2.0 (Table 6). The unstable nature of the compounds at highly acidic pH indicates that the compound may be prone to non-enzymatic degradation, such as oxidation, hydrolysis, and photodegradation. Omeprazole and propantheline were used as respective low and stable reference compounds for pH 2.0 and pH 10.

Bidirectional Permeability Evaluation

Caco-2 cell monolayer permeability evaluation is one of the most physiologically relevant models to understand the permeability of drug candidates and achieve insights into its efflux.³⁶ Control compounds, i.e., propranolol and atenolol showed high and low permeability, respectively, which can rank the tested compounds by their respective Papp values. Test compounds **7a** and **7b** showed moderate permeability. However, **7m** showed low permeability. Compound **7e** was highly permeable among all four tested molecules (Table 7). It was encouraging to see that the majority of the test compounds showed moderate to high permeability, thus making them suitable for oral drug development.

Table 6 Chemical Stability of Test Compounds

Compound ID	Chemical Stability - Half-Life (Min)	
	pH 2.0	pH 10.0
7a	15.2 ± 5.2	52.7 ± 12.4
7b	26.2 ± 7.5	46.1 ± 8.3
7e	10.4 ± 5.7	34.3 ± 7.3
7m	21.2 ± 7.3	39.2 ± 8.7
Omeprazole	10.2 ± 3.1	55.3 ± 11.4
Proprantheline	82.9 ± 14.8	8.3 ± 2.6

Notes: Data represented as mean ± standard deviation; N = 3, Half-life determined using one-phase exponential decay parameter by GraphPad prism software.

Table 7 Bidirectional Permeability of Test Compounds

Compound ID	Bi-Directional CACO ₂ Permeability	
	Papp (Apical to Basal) x 10 ⁻⁶ cm/s	Papp (Basal to Apical) x 10 ⁻⁶ cm/s
7a	9.3 ± 3.1	7.9 ± 2.3
7b	6.4 ± 1.5	4.2 ± 0.9
7e	17.3 ± 2.9	9.9 ± 3.1
7m	2.4 ± 1.7	3.9 ± 1.9
Propranolol	29.0 ± 1.2	21.1 ± 0.3
Atenolol	1.4 ± 0.2	3.0 ± 0.2

Note: Data represented as mean ± SD; N = 3.

Discussion

Macromolecules typically undergo fluctuation after molecular dynamics, which can be well understood from their end-stage conformation and helps us know protein-ligand interactions. During the molecular dynamics study, it was observed that overall, the EGFR-ligand complexes with **7a**, **7b**, **7e**, and **7m** were found to be stable. Further, from Figure 3, it was also confirmed that the kinase hinge residues are essential for binding the small molecules to the EGFR protein; this could possibly be due to the helix region near the loops and hinge region.¹⁷ Given the phenomenon wherein, upon binding with ligands, the loop region that undergoes conformational change is captured as fluctuation in Figure 5. Overall, the three compounds **7a**, **7b**, and **7m**, form relatively stable complexes with low fluctuations and higher compactness with EGFR than **7e**, which aligned with our experimental results. During an in-vitro cell viability study using LDH assay, the anti-proliferative activity of these four compounds against EGFR expressing MCF7 cells was confirmed, which was earlier reported in our previous studies.¹⁵ The most active compound, **7a**, retained the H-bonds and was found to form a most stable protein-ligand complex, as evident by its low RMSD and RMSF values.

In correlation with molecular dynamic study results, three test compounds showed significant inhibition of EGFR^{WT} kinase activity. At the same time, the mutant EGFR^{T790M} was not that efficient, showing target-specific activities of **7a**, **7b**, and **7m** which weaken when the molecular target is mutated. Moreover, none of these compounds showed any significant inhibition on healthy lung fibroblast cell line MRC5, which emphasizes target-driven activity, which was further evident by EGFR kinase activity assay using EGFR^{WT} and EGFR^{T790M}.

Lastly, the solubility and Log D results of three compounds (**7a**, **7b**, and **7m**) were suitable for developing orally administered drugs therapeutically to promote intestinal absorption. Compound **7e** was found to be highly lipophilic, making its development challenging. Thus, it is advisable to structurally modify it to retain its binding affinity and pharmacological activity while improving the drug-like properties. More than 60 min of stability for all four test compounds in the plasma matrix from mice and humans would help during pre-clinical and clinical pharmacokinetics studies by ensuring negligible ex-vivo degradation during analysis. In liver microsomal stability, the compounds follow the phase-1 metabolism pathway. They are relatively more stable in higher species than the rodent (mouse) except **7b**, which offers almost the same metabolism in both species. The test compounds are unstable at a highly acidic pH, which can be addressed by suitable structural modification or formulation approaches such as enteric coating, to achieve desired pharmacokinetic exposure at a later stage of drug development.

Conclusion

We show here that about 1500 1,2,4-oxadiazole derivatives were designed through in-silico tools as ATP mimicking tyrosine kinase inhibitors of EGFR. Of them, four molecules (**7a**, **7b**, **7e**, and **7m**) showed good in-vitro IC₅₀ values in EGFR expressing MCF7 cells. Apart from EGFR^{WT}, the compounds also showed encouraging inhibitory activity against mutant EGFR^{T790M} with IC₅₀ values of <10 and <50 micromolar. Molecular dynamics studies revealed that the most active compound, **7a** retained the H-bonds for a more extended period and formed a stable protein-ligand complex, as evident by its low RMSD and RMSF values. Compound **7e** showed the highest fluctuation and lesser number of hydrogen bonds which explains the lower activity of this compound.

Further, in-vitro ADME data indicate a good correlation between solubility, lipophilicity, and permeability of these compounds. These data were encouraging as good physicochemical properties are essential for designing formulation approaches for the oral delivery of these compounds at further stages of development. Also, excellent stability at 37 °C will enable efficient storage and shipment of plasma samples from any study at later stages of development. None of the compounds showed extensive metabolism in the tested species indicating the advantage of higher oral bioavailability at a later stage of the development. The excellent stability of the compounds at alkaline pH with susceptibility towards acidic pH needs to be considered to develop a suitable formulation for better oral delivery. Also, there is an excellent opportunity to further improve the stability of these compounds by appropriate salt screening.

Disclosure

Vishal Unadkat and Shishir Rohit are employees of Kashiv Biosciences Pvt Ltd, Ahmedabad 382210, Gujarat, India. Vinod Sanna is an employee of Piramal Pharma Solutions, Ahmedabad, 382213, Gujarat, India. The authors report no other potential conflicts of interest for this work.

References

1. Housman G, Byler S, Heerboth S, et al. Drug resistance in cancer: an overview. *Cancers*. 2014;6(3):1769–1792. doi:10.3390/cancers6031769
2. Kamath S, Buolamwini JK. Targeting EGFR and HER-2 receptor tyrosine kinases for cancer drug discovery and development. *Med Res Rev*. 2006;26(5):569–594. doi:10.1002/med.20070
3. Arteaga CL. The epidermal growth factor receptor: from mutant oncogene in nonhuman cancers to therapeutic target in human neoplasia. *J Clin Oncol*. 2001;19(18Suppl):32S–40S. doi:10.1159/000093092
4. Herbst RS. Review of epidermal growth factor receptor biology. *Int J Radiat Oncol Biol Phys*. 2004;59(2 Suppl):21–26. doi:10.1016/j.ijrobp.2003.11.041
5. Liang Y, Zhang T, Zhang J. Natural tyrosine kinase inhibitors acting on the epidermal growth factor receptor: their relevance for cancer therapy. *Pharmacol Res*. 2020;161:105164. doi:10.1016/j.phrs.2020.105164
6. Lynch TJ, Bell DW, Sordella R, et al. Activating mutations in the epidermal growth factor receptor underlying responsiveness of non-small-cell lung cancer to gefitinib. *N Engl J Med*. 2004;350(21):2129–2139. doi:10.1056/NEJMoa040938
7. Pao W, Chmielecki J. Rational, biologically based treatment of EGFR-mutant non-small-cell lung cancer. *Nat Rev Cancer*. 2010;10(11):760–774. doi:10.1038/nrc2947
8. King CR, Kraus MH, Aaronson SA. Amplification of a novel v-erbB-related gene in human mammary carcinoma. *Science*. 1985;229(4717):974–976. doi:10.1126/science.2992089
9. Juan O, Popat S. Treatment choice in epidermal growth factor receptor mutation-positive non-small-cell lung carcinoma: latest evidence and clinical implications. *Ther Adv Med Oncol*. 2017;9(3):201–216. doi:10.1177/1758834016687262
10. Kannaiyan R, Mahadevan D. A comprehensive review of protein kinase inhibitors for cancer therapy. *Expert Rev Anticancer Ther*. 2018;18(12):1249–1270. doi:10.1080/14737140.2018.1527688
11. Zhao J, Zhang T, Liang Y, Zou H, Zhang J. Inhibitory activities of 20 (R, S)-protopanaxatriol against epidermal growth factor receptor tyrosine kinase. *Food Chem Toxicol*. 2021;155:112411. doi:10.1016/j.fct.2021.112411
12. Schuster D, Laggner C, Langer T. Why drugs fail—a study on side effects in new chemical entities. *Curr Pharm Des*. 2005;11(27):3545–3559. doi:10.2174/138161205774414510
13. Segall MD, Beresford AP, Gola JM, Hawksley D, Tarbit MH. Focus on success: using a probabilistic approach to achieve an optimal balance of compound properties in drug discovery. *Expert Opin Drug Metab Toxicol*. 2006;2(2):325–337. doi:10.4103/0973-1296.176111
14. Gill AL, Verdonk M, Boyle RG, Taylor R. A comparison of physicochemical property profiles of marketed oral drugs and orally bioavailable anti-cancer protein kinase inhibitors in clinical development. *Curr Top Med Chem*. 2007;7(14):1408–1422. doi:10.2174/156802607781696819
15. O'Brien Z, Fallah Moghaddam M. Small-molecule kinase inhibitors approved by the FDA from 2000 to 2011: a systematic review of pre-clinical ADME data. *Expert Opin Drug Metab Toxicol*. 2013;9(12):1597–1612. doi:10.1517/17425255.2013.834046
16. Meanwell NA. Improving drug candidates by design: a focus on physicochemical properties as a means of improving compound disposition and safety. *Chem Res Toxicol*. 2011;24(9):1420–1456. doi:10.1021/tx200211v
17. Bain J, Plater L, Elliott M, et al. The selectivity of protein kinase inhibitors: a further update. *Biochem J*. 2007;408(3):297–315. doi:10.1042/BJ20070797
18. Kitagawa D, Yokota K, Gouda M, et al. Activity-based kinase profiling of approved tyrosine kinase inhibitors. *Genes Cells*. 2013;18(2):110–122. doi:10.1111/gtc.12022
19. Yamamoto N, Honma M, Suzuki H. Off-target serine/threonine kinase 10 inhibition by Erlotinib enhances lymphocytic activity leading to severe skin disorders. *Mol Pharmacol*. 2011;80(3):466–475. doi:10.1124/mol.110.070862
20. Voigtlaender M, Schneider-Merck T, Trepel M. Lapatinib. *Rec Res Cancer Res*. 2018;211:19–44. doi:10.1007/978-3-319-91442-8_2
21. Ren JX, Li LL, Zheng RL, et al. Discovery of novel Pim-1 kinase inhibitors by a hierarchical multistage virtual screening approach based on SVM model, pharmacophore, and molecular docking. *J Chem Inf Model*. 2011;51(6):1364–1375. doi:10.1021/ci100464b
22. Umar BA, Uzairu A, Shallangwa GA, Uba S. Rational drug design of potent v600e-braf kinase inhibitors through molecular docking simulation. *J Eng Exact Sci*. 2019;5:0469–0481. doi:10.18540/jcecv15iss5pp0469-0481
23. Choowongkamon K, Sawatdichaikul O, Songtawee N, Limtrakul J. Receptor-based virtual screening of EGFR kinase inhibitors from the NCI diversity database. *Molecules*. 2010;15(6):4041–4054. doi:10.3390/molecules15064041

24. Unadkat V, Rohit S, Parikh P, Sanna V, Singh S. Rational design-aided discovery of novel 1, 2, 4-oxadiazole derivatives as potential EGFR inhibitors. *Bioorg Chem.* 2021;105124. doi:10.1016/j.bioorg.2021.105124
25. Unadkat V, Rohit S, Parikh P, Sanna V, Singh S, Patel K. Corrigendum to “Rational design-aided discovery of novel 1,2,4-oxadiazole derivatives as potential EGFR inhibitors” [*Bioorg Chem.* 114 (2021) 105124]. *Bioorg Chem.* 2021;117:105459. doi:10.1016/j.bioorg.2021.105459
26. Parikh PH, Timaniya JB, Patel MJ, Patel KP. Design, synthesis, and characterization of novel substituted 1,2,4-oxadiazole and their biological broadcast. *Med Chem Res.* 2020;29:538–548. doi:10.1007/s00044-020-02505-8
27. Ryckaert J-P, Ciccoliti G, Berendsen HJ. Numerical integration of the cartesian equations of motion of a system with constraints: molecular dynamics of n-alkanes. *J Comput Phys.* 1977;23(3):327–341. doi:10.1016/0021-9991(77)90098-5
28. Chinnasamy K, Saravanan M, Poomani K. Evaluation of binding and antagonism/downregulation of brilanestrant molecule in estrogen receptor- α via quantum mechanics/molecular mechanics, molecular dynamics and binding free energy calculations. *J Biomol Struct Dyn.* 2020;38(1):219–235. doi:10.1080/07391102.2019.1574605
29. Suda K, Onozato R, Yatabe Y, Mitsudomi T. EGFR T790M mutation: a double role in lung cancer cell survival? *J Thorac Oncol.* 2009;4:1–4. doi:10.1097/JTO.0b013e3181913c9f
30. Alsenz J, Kansy M. High throughput solubility measurement in drug discovery and development. *Adv Drug Deliv Rev.* 2007;59(7):546–567. doi:10.1016/j.addr.2007.05.007
31. Di L, Kerns EH. Profiling drug-like properties in discovery research. *Curr Opin Chem Biol.* 2003;7(3):402–408. doi:10.1016/s1367-5931(03)00055-3
32. Kerns EH, Di L. Pharmaceutical profiling in drug discovery. *Drug Discov Today.* 2003;8(7):316–323. doi:10.1016/s1359-6446(03)02649-7
33. Di L, Kerns EH, Hong Y, Chen H. Development and application of high throughput plasma stability assay for drug discovery. *Int J Pharm.* 2005;297(1–2):110–119. doi:10.1016/j.ijpharm.2005.03.022
34. Obach RS. Prediction of human clearance of twenty-nine drugs from hepatic microsomal intrinsic clearance data: an examination of in vitro half-life approach and nonspecific binding to microsomes. *Drug Metab Dispos.* 1999;27(11):1350–1359.
35. Di L, Kerns EH, Chen H, Petusky SL. Development and application of an automated solution stability assay for drug discovery. *J Biomol Screen.* 2006;11(1):40–47. doi:10.1177/1087057105281363
36. Wang Z, Hop CE, Leung KH, Pang J. Determination of in vitro permeability of drug candidates through a caco-2 cell monolayer by liquid chromatography/tandem mass spectrometry. *J Mass Spectrom.* 2000;35(1):71–76. doi:10.1002/(SICI)1096-9888(200001)35:1<71::AID-JMS915>3.0.CO;2-5

OncoTargets and Therapy

Dovepress

Publish your work in this journal

OncoTargets and Therapy is an international, peer-reviewed, open access journal focusing on the pathological basis of all cancers, potential targets for therapy and treatment protocols employed to improve the management of cancer patients. The journal also focuses on the impact of management programs and new therapeutic agents and protocols on patient perspectives such as quality of life, adherence and satisfaction. The manuscript management system is completely online and includes a very quick and fair peer-review system, which is all easy to use. Visit <http://www.dovepress.com/testimonials.php> to read real quotes from published authors.

Submit your manuscript here: <https://www.dovepress.com/oncotargets-and-therapy-journal>